JACS
JOURNAL OF THE AMERICAN CHEMICAL SOCIETY

ARTICLE

pubs.acs.org/JACS

Influence of Electric Field on SERS: Frequency Effects, Intensity Changes, and Susceptible Bonds

Sharath Sriram,*[,†] Madhu Bhaskaran,[†] Shijian Chen,[‡] Sasani Jayawardhana,[§] Paul R. Stoddart,[§] Jefferson Z. Liu,[⊥] Nikhil V. Medhekar,*[,‡] Kourosh Kalantar-Zadeh,[†] and Arnan Mitchell[†]

[†]Microplatforms Research Group, School of Electrical and Computer Engineering, RMIT University, Melbourne, Australia
[‡]Department of Materials Engineering and [⊥]Department of Mechanical Engineering, Monash University, Clayton, Australia
[§]Faculty of Engineering and Industrial Science, Swinburne University of Technology, Hawthorn, Australia

Supporting Information

ABSTRACT: The fundamental mechanism proposed to explain surface-enhanced Raman scattering (SERS) relies on electromagnetic field enhancement at optical frequencies. In this work, we demonstrate the use of microfabricated, silver nanotextured electrode pairs to study, in situ, the influence of low frequency (5 mHz to 1 kHz) oscillating electric fields on the SERS spectra of thiophenol. This applied electric field is shown to affect SERS peak intensities and influence specific vibrational modes of the analyte. The applied electric field perturbs the polar analyte, thereby altering the scattering cross section. Peaks related to the sulfurous bond which binds the molecule to the silver nanotexture exhibit strong and distinguishable responses to the applied field, due to varying bending and stretching mechanics. Density functional theory simulations are used to qualitatively verify the experimental observations. Our experimental and simulation results demonstrate that the SERS spectral changes relate to electric field induced molecular reorientation, with dependence on applied field strength and frequency. This demonstration creates new opportunities for external dynamic tuning and multivariate control of SERS measurements.

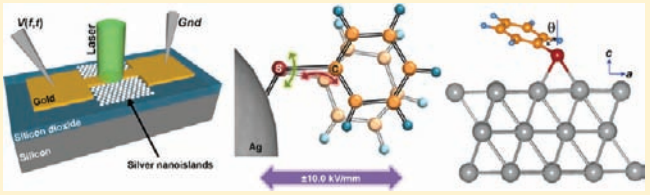

INTRODUCTION

Surface-enhanced Raman scattering (SERS) is a technique that provides greatly enhanced sensitivity for analytes adsorbed onto nanostructured metal(ized) surfaces. The fundamental technique was discovered over 30 years ago,[1,2] and the advent of nanolithography and nanoimprint technologies has allowed SERS to be explored more widely in the past decade. SERS surfaces are typically coated with gold or silver nanoparticles, with the nanostructuring achieved either by photolithography,[3] nanoimprint lithography,[4−6] electrochemistry,[7,8] shadowing,[9] nanosphere lithography,[10] indentation,[11] or the use of a substrate with an inherent or reactively synthesized nanotexture.[12−14] Demonstrations of SERS have shown million-fold increases in the intensity of Raman spectra, but are yet to achieve reliable detection of trace and multiple analytes.[1] SERS has been extensively investigated for nondestructive detection of low concentrations of organic chemical compounds. Many recent investigations have focused on the detection of biomolecules and harmful trace chemicals (water contaminants, explosive agents, etc.).[2,15−18]

The current mechanism proposed to explain the SERS effect relies on a combination of chemical and electromagnetic field enhancement at the surface of the metal to which the analyte is adsorbed.[1,2,19] At visible and infrared wavelengths, light can become trapped at the surface of metals such as silver and gold in the form of a surface plasmon. Nanoscale metal features can act as optical resonators, vastly concentrating the optical field strength close to the metal surface. Thus, when a SERS substrate is illuminated with intense laser radiation, certain nanofeatures on the surface resonate and concentrate the light in so-called 'hot spots'. Molecules adsorbed or in close proximity to these 'hot spots' experience an exceptionally large electromagnetic field and the probability of Raman scattering is greatly increased. Since optical plasmons are polarized with electric field normal to the metal surface, molecular vibrations that are also aligned normal to the metal surface are selectively enhanced.[1,2]

The SERS process is determined by the interactions between the optical excitation and the analyte, and the resulting electromagnetic enhancement. Insight into this correlation is critical for fundamental understanding of SERS and the creation of highly selective SERS sensors. Given the dominance of polarized electromagnetic enhancement in plasmonics and SERS, any external polarizing electric field (additional excitation source) can be expected to influence the SERS enhancement process.

In this work, we report on the impact of modulating analytes linked to nanotextures by an externally applied oscillating electric field. The use of this oscillating field in combination with SERS sensing, creates a multivariate external control capability, by adding field strength and frequency to the SERS accumulation parameters.

Received: September 21, 2011
Published: November 16, 2011

dx.doi.org/10.1021/ja208893q | J. Am. Chem. Soc. 2012, 134, 4646–4653

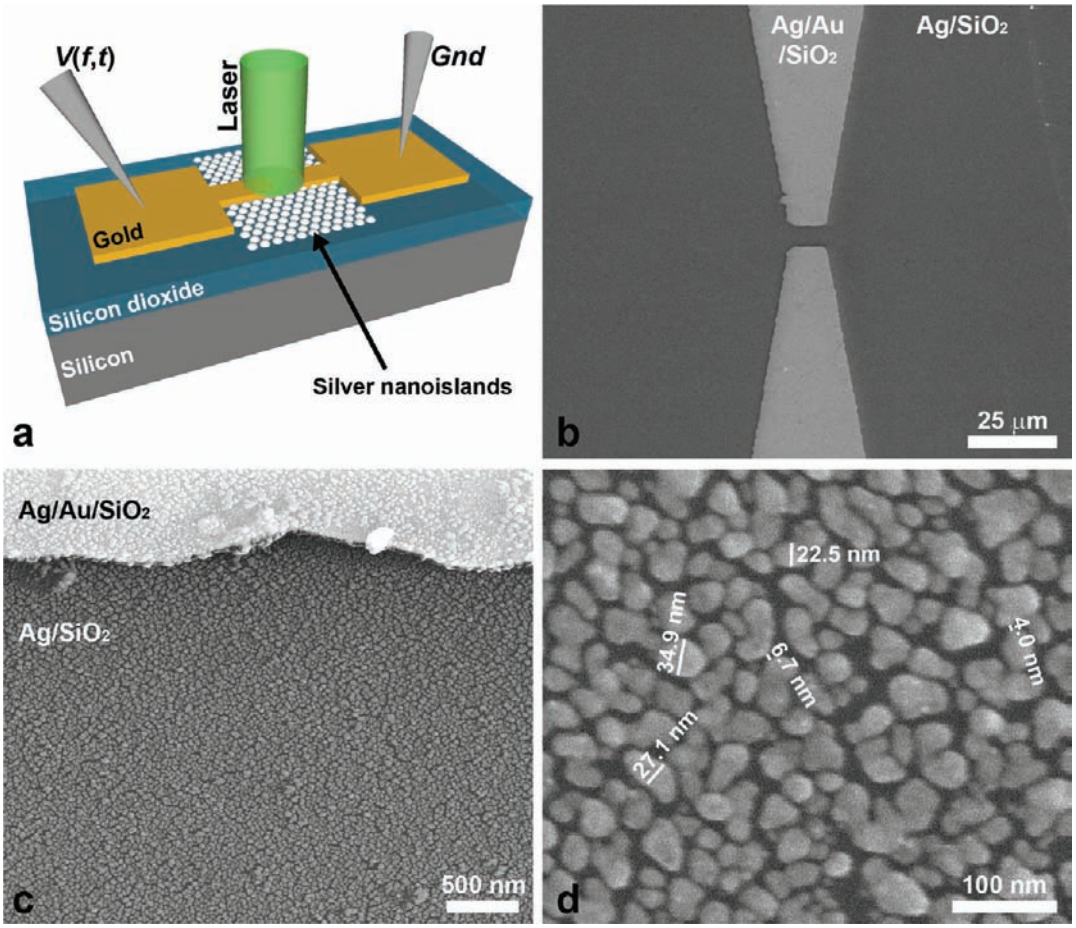

Figure 1. Schematic of the microfabricated device and in situ SERS measurement arrangement is shown in panel a (not to scale). Scanning electron micrographs of a microfabricated gold electrode pair, nanotextured silver coating on the electrode, and discrete 20−40 nm silver nanoislands are shown in panels b−d, respectively.

This novel approach can potentially serve as a platform to selectively enhance vibrational modes using a combination of these electronic input parameters. This work first describes the realization and testing of electrode pair integrated SERS microdevices.

The correlation between observed electric field dependent spectral trends with analyte vibration modes is then discussed. Finally, first principle theoretical techniques are utilized to explore field dependent analyte structure and qualitatively support experimental observations.

RESULTS AND DISCUSSION

The experimental apparatus consisted of a nanotextured, metalized surface to achieve SERS, with an integrated microscale electrode pair for applying the external field as shown in Figure 1a. Oxidized silicon substrates were coated with a 100 nm gold layer, which was patterned to define electrode pairs with spacings of 2 and 4 μm (Figure 1b). A SERS-active texture of silver nanoislands was deposited using an oblique angle deposition (OAD) process.[20] The substrates were placed with an angle of 86° between the sample normal and the vapor flux, resulting in an insulating film of discrete silver nanoislands of about 20−40 nm in diameter (Figure 1c,d); therefore, no current flow during application of the external electric field was observed. These samples were dip coated for monolayer functionalization in a 10 mM ethanolic solution of thiophenol.

To test the influence of an external electric field on the SERS response, the functionalized electrode pair samples were measured using a Raman microscope. During Raman measurements, an oscillating voltage was applied across the electrode pair on either side of the nanoisland array. It should be noted that no static (i.e., direct current) fields were applied for two reasons: (i) static fields are known to electrochemically degrade silver nanostructures and result in the dissociation of the adsorbed analytes[21−23] and (ii) the motivation of this work is to develop a platform for SERS enhancement with multivariate parametric control, by adding the strength, frequency, and phase of an external electric field to the SERS accumulation parameters. The method of testing is also illustrated in Figure 1a. Reference SERS spectra were collected regularly with no electric field influence (these served as control experiments). This data was used for normalizing the results when further measurements were taken upon applying an electric field. The wavenumber and intensity of five peaks with different bond structure assignment were selected for further analysis, due to either their representative or anomalous behavior.[24] These five peaks of thiophenol and their associated vibrational modes are presented in Table 1.

Sinusoidal fields which oscillated between ±10 and ±20 V were applied across the 4 μm spacing and ±20 V across the 2 μm spacing, with resulting maximum field strengths being ±2.5, ±5.0, and ±10.0 kV/mm, respectively. The frequency of the applied

fields was scanned from 5 mHz to 1 kHz. All as-collected SERS spectra are presented in Figure S1 in the Supporting Information.

Table 1. Assignment of Vibrational Modes for Thiophenol Raman Peaks[24,a]

Raman shifts (cm^{-1})		
theoretical[24]	experimental	vibrational mode (s)
1076	1070	C−C asymmetric stretching
1018	1019	Ring in-plane deformation and C−C symmetric stretching
990	997	Ring out-of-plane deformation and C−H out-of-plane bending
471	462	C−S out-of-plane bending
404	420	C−S stretching and ring in-plane deformation

[a] Only the peaks relevant to this work are listed.

Figure 2a presents a reference spectrum obtained with no applied field. The significant peaks and their associated bond structure are labeled. Figure 2b−d presents the normalized intensity of the five significant SERS peaks of thiophenol as a function of the frequency of the applied electric field for three different field strengths (also see Tables S1−S3).

The background-subtracted, normalized SERS intensity for the 1070, 1019, and 997 cm^{-1} peaks decrease in a simple gradual manner with frequency, while the peaks at 420 and 462 cm^{-1} exhibit a more complex response (discussed later) to changes in frequency and amplitude of the applied field.

It is perhaps surprising that there should be any dependence of the Raman response on the frequency of the applied electric field, since at the low frequencies under study, the fields could be considered *quasi*-static. It should be noted that the acquisition time was 50 s, so a complete cycle is only recorded for frequencies exceeding 20 mHz; and thus, the number of electric field oscillations that are averaged change dramatically over the range of frequencies investigated. The strength of the applied field may also reduce due to changing dielectric properties and the

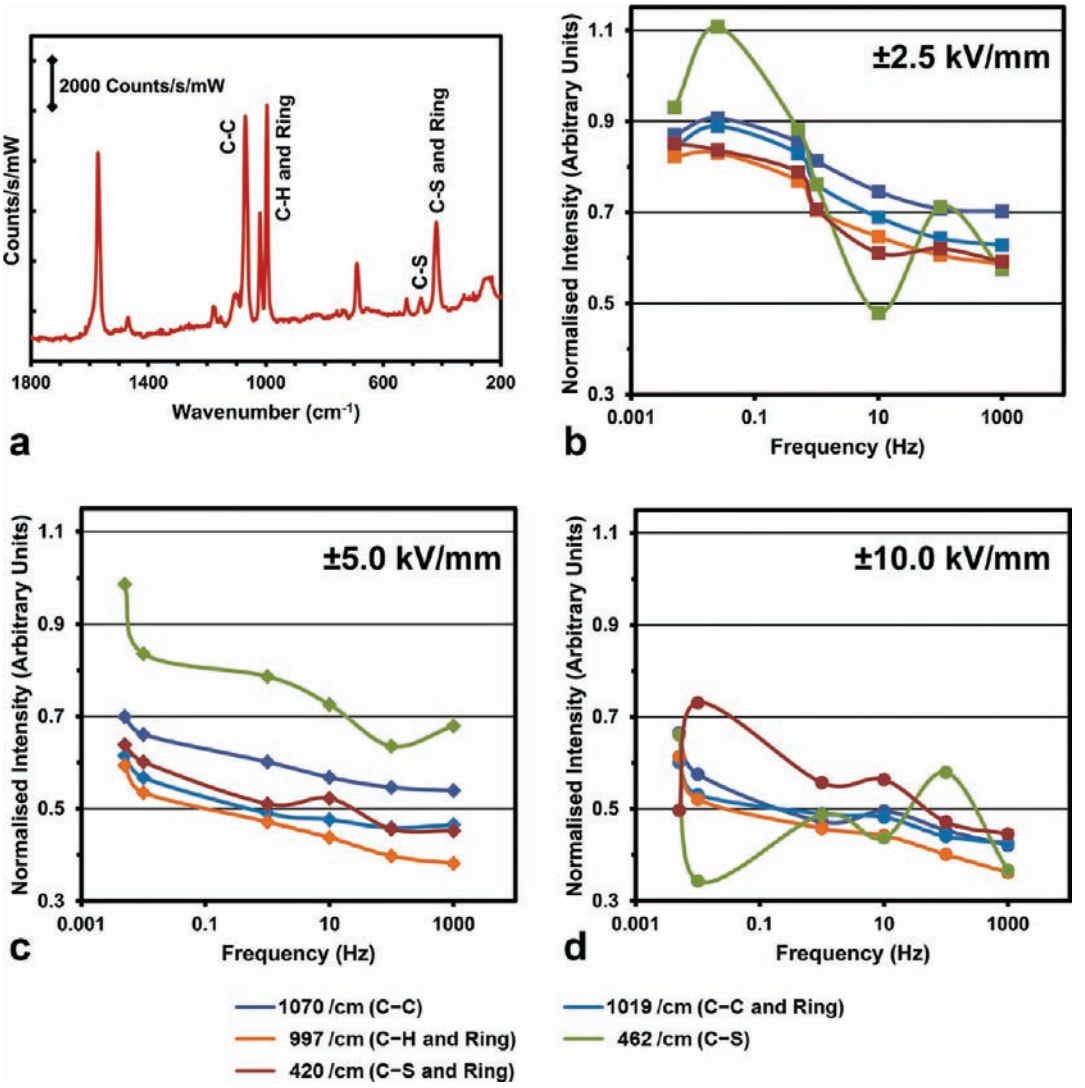

Figure 2. (a) Reference SERS spectrum for thiophenol measured with no electric field. The trends in relative peak intensity for five significant peaks at different frequencies, normalized to the case of no electric field, is shown for electric fields oscillating between (b) ±2.5 kV/mm, (c) ±5.0 kV/mm, and (d) ±10.0 kV/mm.

dx.doi.org/10.1021/ja208893q | *J. Am. Chem. Soc.* 2012, 134, 4646–4653

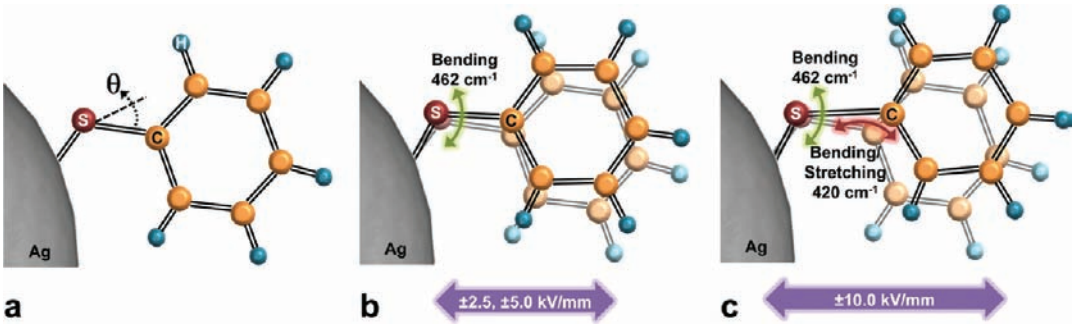

Figure 3. Electric field induced thiophenol molecular kinetics. (a) Schematic representation of typical thiophenol binding to silver nanostructures. (b) The anchoring C−S bond of thiophenol subject to bending forces (related to the 462 cm^{-1} peak) at lower electric field strengths. (c) Higher electric fields subject the thiophenol molecule to stronger bending and potential stretching forces (related to the 420 cm^{-1} peak). (Not to scale.)

impedance and resistive behavior of the microelectrode structure and also the cabling and analysis instruments. All of these effects could be used to explain the observed gradual reduction in resulting in a corresponding reduction in the observed Raman peaks.

It is hard, however, to use such arguments to explain the complex behavior of the peaks at 420 and 462 cm^{-1}. It could be suggested that the observation of this incongruous behavior of the peak at 462 cm^{-1} is due to it being of a low intensity level and thus could be adversely influenced by noise. However, careful analysis of the peaks shows that the noise level is negligible. Moreover, it should be noted that the 420 cm^{-1} peak also exhibits incongruous behavior, yet it is a relatively strong peak in the spectrum with >3000 counts/(s/mW) which is far stronger than other peaks with monotonic trends.

Further, the observed gradual response of the 1070, 1019, and 997 cm^{-1} peaks and the more complex response of the 420 and 462 cm^{-1} peaks cannot be explained by known phenomena such as the charge transfer mechanisms[21,23,25] or the vibrational Stark effect.[26,27] The former results in large frequency or wavenumber shifts while the latter causes significant peak broadening, both of which were not observed in the SERS spectra resulting from our experiments. It should also be noted that spectral fluctuations, especially changes in relative intensities of vibrational modes, have been observed in gap-mode tip enhanced Raman spectroscopic (TERS) measurements.[28,29] These are often attributed to changes in electromagnetic enhancement due to variations in tip−sample spacing as a result of surface roughness and scanning parameters.[28−32] These spacing dependent outcomes have been shown to relate to the TERS enhancement factor, with selective peak enhancement dependent on the location of the tip relative to bond positions.[30]

Thiophenol is a polar molecule consisting of a benzene ring with a sulfur tether that is bound to the nanostructured silver surface by hydrogen replacement to form an Ag−S bond. Previous works by Carron and Hurley[33] and Mani et al.[34] have shown that the thiophenol monolayer stabilizes in an erect configuration with the anchoring C−S bonds at specific angles θ to the normal (Figure 3a), which depends on the surface orientation and location of the molecule on the metal surface.

We propose that under the influence of an oscillating electric field, the thiophenol molecules are forced to constantly realign their net polarization with respect to the direction (polarity) of the electric field. The manner in which the molecules are expected to respond to the oscillating electric field is presented in Figure 3, panels b and c, for modest and large electric fields, respectively. The benzene ring itself remains undistorted and simply realigns in response to the electric field. The bonds associated with the sulfur tether must however bend and distort in order to allow the benzene ring to realign.

This hypothesis is supported by our experimental observations. The realignment of the benzene ring will determine the molecular bonds which are aligned with the polarization of surface plasmon excited by the incident laser with maximum Raman scattering observed for only part of the oscillation cycle. For the incident green laser (532 nm), the maximum spectral response will be for bonds aligned normal to the substrate surface, based on the selection rules proposed by Moskovits and Suh.[35] Static electric field dependent surface selection rules have also recently been proposed for quantum dot systems.[36]

The response of the peaks to the applied field strength is also of interest. The behavior of the 420 and 462 cm^{-1} peaks are significantly different from that of the three peaks at 1070, 1019, and 997 cm^{-1}, which do not change form with increasing field strength (Figure 2b−d). The 462 cm^{-1} peak rises and falls dramatically with increasing frequency of the external field for all field strengths investigated. The 420 cm^{-1} peak only shows mild differences from the three benzene ring peaks for lower electric fields (Figure 2b,c). At the highest electric field strength, the variations in the intensity of the 420 cm^{-1} peak with frequency are more apparent.

This behavior of the 420 and 462 cm^{-1} peaks can be explained by considering the specific bond symmetry generating the SERS peaks. The 462 cm^{-1} peak corresponds to the bending modes of the C−S(−Ag) bond tethering the thiophenol to the silver nanostructure surface and the 420 cm^{-1} peak is a result of the stretching of the C−S bond and/or the deformations of the benzene ring. Figure 3 presents an illustration of what may occur when thiophenol is exposed to an external electric field. Figure 3a presents the situation with no external electric field, where the C−S bond is aligned at an angle θ to the normal to the silver surface. When an oscillating field is applied across the silver island, the field strength normal to the surface will increase (as the electric field lines are always normal to a conductive surface). This will result in rotation of the benzene ring and the C−S bond to align with the field as shown in Figure 3b. At lower electric field strengths (2.5 and 5.0 kV/mm), the benzene ring can realign to compensate for this applied field through bending of the C−S bond. At the higher electric field (10.0 kV/mm), the C−S bond resists further bending and the bond and the benzene ring itself may deform in the direction of the applied field to achieve equilibrium as shown in Figure 3c. The bending of the C−S bond

dx.doi.org/10.1021/ja208893q | J. Am. Chem. Soc. 2012, 134, 4646–4653

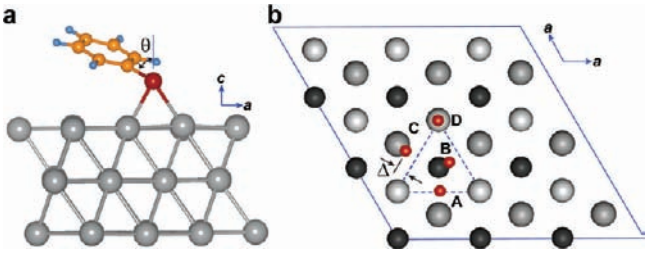

Figure 4. Optimized geometry of a single thiophenolate (C_6H_5S) molecule adsorbed on Ag(111) surface as obtained by density functional theory calculations. (a) Side view shows thiophenolate adsorbed in bridge configuration, with θ being the angle between the C−S bond and the Ag(111) surface normal. Gray, orange, red, and blue spheres denote Ag, C, S, and H atoms, respectively (as in Figure 3). (b) Stable and unique configurations for the adsorption of thiophenolate on Ag(111) can be identified based on the different surface adsorption sites for S atom of the thiophenolate molecule. Top view shows adsorption sites for S atom for four configurations: A (bridge), B (*fcc*-bridge), C (*hcp*-bridge), and D (top). Light, medium, and dark gray spheres indicate Ag atoms in topmost, second, and third layers, respectively, while red spheres denote adsorption sites of the S atom. Δ indicates the projected offset distance for the S atom from the closest bridge site. The thiophenolate molecule (other than the S atom) is not shown for clarity.

influences the 462 cm^{-1} peak. The deformation of the C−S bond and orientation changes of the benzene ring influences the 420 cm^{-1} peak. The bending of the C−S bond and the resulting deformations of the tethered benzene ring under a strong applied field are inter-related. This may explain the behavior of the 420 and 462 cm^{-1} peaks observed for a large applied field in Figure 2d. Such bond bending or ring deformation dependent changes to normalized Raman scattering intensity have been observed in plasmon resonances due to bending kinetics in DNA.[37,38] These results highlight that the spectral variations are strongly correlated to field-induced molecular reorientation, and the relationship between the molecular orientation and the electromagnetic field of the incident laser.

To test this interpretation of the experimental observations, we have performed first-principles density functional theory (DFT) calculations to study how an applied electric field influences the adsorption geometry of thiophenols on metallic surfaces. It is well-known that for aromatic phenols adsorbed on high symmetry metallic surfaces, the adsorption patterns are highly dependent on the chemical structure of the adsorbent molecules, surface coverage, and the method of preparation.[39] For instance, oligobenzenethiols form a well-ordered self-assembled monolayer on Au(111) with a $(2\sqrt{3} \times \sqrt{3})$ $R30°$ periodic symmetry. For thiophenols, it has been suggested that the formation of an ordered monolayer depends on the method of preparation.[40] Moreover, metallic surfaces can act as a catalyst for the dissociation of phenols (X−SH) to form phenolates (X−S), which then chemically bind to the surface through strong covalent interactions.[41]

In light of these experimental observations, we consider a model system with an isolated thiophenolate molecule adsorbed on Ag(111) surface for our DFT studies (see Methods section for details). Our simulation cell consisted of a 3 × 3 Ag(111) surface unit cell and three Ag layers forming a slab. Isolated thiophenolate molecules were initially placed in the vicinity of the surface in various configurations and their optimized geometries were obtained for external electric fields in the range of −0.5 to +0.5 eV/Å.

Table 2. The Adsorption Energy E_a and Structural Parameters for the Stable Configurations of Thiophenolate on a Ag(111) Surface in the Absence of an External Electric Field[a]

configuration	E_a (eV)	r{S−Ag} (Å)	Δ (Å)	θ (deg)
bridge	1.597	2.59	0.00	66.8
fcc-bridge	1.584	2.58	0.33	60.0
hcp-bridge	1.562	2.60	0.41	60.7
top	1.312	2.47	-	75.7

[a] As indicated in Figure 4, r, Δ, and θ denote the S−Ag bond length, the projected offset distance for the S atom from the closest bridge site, and the angle between the S−C bond and the surface normal, respectively.

After relaxation, the thiophenolate molecule adsorbs in four unique configurations irrespective of the external electric field. Each of these configurations can be characterized by the location of the thiophenolate S atom relative to the Ag atoms in topmost surface layer. These configurations are marked in Figure 4 as follows: (A) bridge, S atom at the bridge site between two surface Ag atoms; (B) *fcc*-bridge, S atom in the bridge site and shifted toward *fcc* stacking sequence; (C) *hcp*-bridge, S atom in the bridge site and shifted toward *hcp* stacking sequence; and (D) top, S atom vertically on top of a surface Ag atom. After complete relaxation for each configuration, we computed the adsorption energy E_a defined as $E_a = -[E_T - E_{Ag+Field} - E_{Molecule}]$, where E_T is the total energy of the supercell containing thiophenolate adsorbed on the Ag surface in the presence of electric field, $E_{Ag+Field}$ is the total energy of pure Ag slab in the same supercell, and $E_{Molecule}$ is the energy of isolated thiophenolate molecule in the same supercell. With this definition, positive adsorption energy denotes that absorption is energetically favorable.

Table 2 shows the adsorption energies and geometrical parameters such as S−Ag bond length r, tilt angle θ, and the offset of the S atom Δ for each configuration in the absence of external electric field. We find that the bridge configuration has the largest adsorption energy. In the bridge configuration, the S atom of thiophenolate is bonded to two surface Ag atoms and the molecule is tilted from the surface normal by 66.8°. With tilt angle close to 60°, *fcc* and *hcp* bridge configurations are structurally very similar to each other except for the location of S atom relative to the surface. Their bonding environment is also similar to the bridge configuration, resulting in slightly lower adsorption energies. Finally, with S atom bonded to only one surface Ag atom, we found that the top site is the least favorable site with E_a of 1.31 eV. It is worth noting that our results on adsorption geometries of isolated thiophenolates on Ag(111) in the absence of electric field as shown in Table 2 are in a qualitative agreement with a recent theoretical study that predicts similar bridge, *fcc*-bridge, *hcp*-bridge, and top configurations for thiophenolate adsorbed on Au(111).[39] However, in contrast to the Au(111) surface, it appears that configurations with thiophenols adsorbed on a Ag(111) surface at *fcc* and *hcp* hollow sites, where the S atom is bonded to three surface atoms, are not stable. Nevertheless, our calculated adsorption energies are in the range of 1.3−1.6 eV, in good agreement with the reported values.[39]

Next, we consider how an external electric field influences the geometry and energetics of thiophenolate adsorbed on Ag(111) surface. We find that for each configuration, the tilting angle, the S−Ag bond length, and the adsorption energy all change in response to the applied electric field. Table 3 illustrates this effect in the case of the bridge configuration, as an example (with results

dx.doi.org/10.1021/ja208893q | *J. Am. Chem. Soc.* 2012, 134, 4646–4653

Table 3. The Influence of the External Electric Field on the Adsorption Energy E_a and the Geometry of Thiophenolate Adsorbed on Ag(111) in Bridge Configuration

external electric field (eV/Å)	E_a (eV)	r{S−Ag} (Å)	θ (deg)
0.50	1.658	2.61	66.5
0.25	1.603	2.60	66.8
0.00	1.597	2.58	66.8
−0.25	1.626	2.57	67.3
−0.50	1.704	2.54	67.9

for the other configurations presented in Table S4 in the Supporting Information). When the applied electric field varies from +0.5 to −0.5 eV/Å, the thiophenolate molecule moves closer to the surface, with the tilt angle increasing from 66.5 to 67.9°, while the S−Ag bond length reduces from 2.61 to 2.54 Å. We also find that while the adsorption energy E_a increases in the presence of electric field in general, it is much larger for negative electric fields compared with the positive electric fields. Thus, these results indicate that the negative electric fields promote stronger covalent interactions between the Ag surface and the thiophenolate, which can be attributed to the increased electron density in the region between the molecule and the surface. Moreover, we find that for thiophenolate adsorbed in *fcc*-bridge, *hcp*-bridge, and top configurations, the effect of external electric fields is essentially similar to the bridge configuration, where the S−Ag bond compresses or stretches while the plane of the benzene ring tilts closer to or away from the surface in response to the alternating external electric field as employed in our experiments (see Supporting Information).

In addition to bond-stretching and tilting of thiophenolate adsorbed in a particular configuration, we find that the alternating electric field can also influence relative stabilities of different configurations. For instance, Table 2 shows that the difference in the adsorption energy of bridge and *hcp*-bridge configurations is 35 meV in the absence of external electric field. However, our calculations indicate that this difference reduces to 22−25 meV with an applied field of ±0.5 eV/Å. Since the population densities of thiophenols adsorbed in various configurations depend on their relative absorption energies, the alternating external field can also promote switching between configurations. As Figure 4 and Table 2 indicate, switching between adsorption configurations involves a significant change in the relative position of the S atom as well as the tilt angle.

It should be noted that for the DFT calculations, we have considered a model system with isolated thiophenolates adsorbed on low-index, defect-free Ag(111) surface. However, the preparation process for Ag nanoislands covered with thiophenols may also stabilize other high-symmetry surfaces such as (100) and (110) with varying degrees of surface coverage and adsorption symmetries.[42,43] These effects are likely to influence the thiophenol adsorption geometry as well as the response to alternating electric fields. Moreover, it has been suggested that the adsorption of thiophenol in large densities on metallic surfaces can induce a significant strain in the topmost surface layer; thereby, promoting the formation of vacancy defects.[44,45] The presence of such defects near the adsorbed molecules can therefore also influence the adsorption geometry. It should also be noted that the SERS spectral signature for the Ag−S vibrational mode is known to be very weak,[29,33,34] which was the case in our experimental results also. Therefore, a direct comparison of experiments and DFT calculations for this Ag−S bond is not viable, but indicates the need to investigate techniques for selectively enhancing this vibrational mode. Nevertheless, our DFT calculations provide a qualitative confirmation of bond stretching and bending in response to alternating electric fields, as proposed to explain the experimental observations.

CONCLUSIONS

To our knowledge, this work presents the first investigation combining microfabricated electrode pairs and silver nanotextures to investigate the influence of an applied electric field on SERS spectra. Application of an external oscillating field to the polar thiophenol molecules appears to reorient them and reduce the scattering cross section leading to a decrease in scattering intensity for modes of the dangling benzene ring, while the asymmetric C−S bond anchoring the benzene ring to the silver has a complex response which depends on both the strength and frequency of the applied field. Electric field influenced modulation of spectra, with reversible behavior, complements innovative plasmonics switching approaches using molecular switching based on reduction−oxidation and mechanical processes.[46,47] The experimental observations and interpretation are qualitatively validated by first principles DFT calculations.

This work has shown that specific bonds could be distinguished, not only by their specific Raman shifts, but also by observing the dependence of the SERS peak intensity on an oscillating external field. This knowledge may enable signal processing to selectively enhance or suppress the spectra resulting from specific bonds, utilizing the strength, frequency, and the phase of the applied field. This ability to dynamically manipulate the Raman spectra of specific bond types in situ adds an extra dimension to the collection and interpretation of spectra with significant opportunity for selective analysis of multiple analytes simultaneously. The application of this technique to the separation of multiple analytes is currently under investigation.

METHODS

Fabrication of Microscale Electrode Pairs. Silicon substrates with 300 nm of thermally grown silicon dioxide were cleaned using solvents, following which electrode pairs were fabricated by lift-off lithography. The electrodes were defined using 100 nm of electron beam evaporated gold (with a 10 nm chromium adhesion layer), with a spacing between the electrode pairs of 2 and 4 μm.

Synthesis of Silver Nanoislands. A layer of silver ∼60 nm thick was deposited on the electrode pairs by thermal evaporation. An oblique angle deposition (OAD) process was employed with substrates placed at 86° to the normal. This resulted in discrete silver nanoislands about 20−40 nm in diameter. The discrete nature of these islands was verified by the measurement of resistivity at the frequencies under investigations, showing that the electrode pairs remained open circuit with no current flow at such conditions.

SERS Measurements and Electrical Actuation. The electrode pair samples coated with silver nanoislands were functionalized with a self-assembled monolayer of thiophenol (10 mM solution in ethanol).[48] SERS measurements were carried out using a 532 nm laser, with 1.1 mW incident power and 50 s accumulation time. A sinusoidal electric field was applied using an Agilent 33220A arbitrary waveform generator across the electrode pair devices to determine the influence of electric field parameters (voltage and frequency) on the SERS spectra. Normalized intensities for the SERS data were calculated based on actual peak intensities relative to background intensities near the peak of interest.

First Principles Density Functional Theory Simulations. Density functional theory (DFT) simulations were performed using the Vienna Ab Initio Simulation Package (VASP).[49] Electron exchange and correlation was described using the generalized gradient approximation of the Perdew-Burke-Ernzerhof form.[50] Core and valence electrons were treated using the projector-augmented wave potentials supplied with VASP.[51] Using DFT methods, first we obtained the optimized lattice constant for *fcc*-Ag crystal to be 4.16 Å, which is within 2% of the experimental value. The simulation supercell designed to study the adsorption of thiophenol on a Ag(111) surface consisted of 3×3 (111) surface unit cell with three layers of Ag forming a slab. A vacuum of 20 Å separated the periodic images of the slab in the direction normal to the surface in order to ensure accurate energy convergence. For geometry optimization, the supercell vectors and all ionic positions were relaxed using a conjugate gradient algorithm until the Hellmann−Feynman forces were less than 0.02 eV/Å. A 500 eV plane wave kinetic energy cutoff was used in each case. A $7 \times 7 \times 1$ Γ-centered Monkhorst-Pack mesh was used to sample the Brillouin zone for relaxation as well as accurate total energy calculations. Finally, the external electric fields in the direction normal to the slabs (as expected for the conductive silver surface) were applied by introducing dipolar sheets at the center of the simulation cell.[52]

■ ASSOCIATED CONTENT

Supporting Information. Additional data including full unprocessed surface-enhanced Raman spectra collected as reference data and under the influence of electric field together with detailed numerical data used to plot background-subtracted, normalized, relative intensity plots. Density functional theory results of electric field induced molecular orientation for different thiophenolate-silver configurations. This material is available free of charge via the Internet at http://pubs.acs.org.

■ AUTHOR INFORMATION

Corresponding Author
sharath.sriram@gmail.com; nikhil.medhekar@monash.edu

■ ACKNOWLEDGMENT

This work was supported by the Australian Research Council (ARC) through project (Discovery Project DP110100262) and infrastructure funding (LE100100215) and in part by the Australian National Fabrication Facility under the National Collaborative Research Infrastructure Strategy. S.S. and M. B. acknowledge ARC Australian Post-Doctoral Fellowships through DP110100262 and DP1092717, respectively. The authors also acknowledge the support from Australia's National Computational Infrastructure. The authors thank Dr. Gorgi Kostovski for assistance with electron microscopy.

■ REFERENCES

(1) Jeanmaire, D. L.; Van Duyne, R. P. *J. Electroanal. Chem.* **1977**, *84*, 1–20.
(2) Moskovits, M. *Rev. Mod. Phys.* **1985**, *57*, 783–826.
(3) Kim, J. H.; Kang, T.; Yoo, S. M.; Lee, S. Y.; Kim, B.; Choi, Y. K. *Nanotechnology* **2009**, *20*, 235302.
(4) Liu, G. L.; Lee, L. P. *Appl. Phys. Lett.* **2005**, *87*, 074101.
(5) Alvarez-Puebla, R.; Cui, B.; Bravo-Vasquez, J.-P.; Veres, T.; Fenniri, H. *J. Phys. Chem. C* **2007**, *111*, 6720–6723.
(6) Wu, W.; Hu, M.; Ou, F. S.; Li, Z.; Williams, R. S. *Nanotechnology* **2010**, *21*, 255502.
(7) Abdelsalam, M. E.; Bartlett, P. N.; Baumberg, J. J.; Cintra, S.; Kelf, T. A.; Russell, A. E *Electrochem. Commun.* **2005**, *7*, 740–744.
(8) Hong, X.; Wang, G.-Z.; Wang, Y.; Zhu, W.; Shen, X.-S. *Chin. J. Chem. Phys.* **2010**, *23*, 596–602.
(9) Liu, F. M.; Green, M. *J. Phys. Chem. B* **2003**, *107*, 13015–13021.
(10) Haynes, C. L.; Van Duyne, R. P. *J. Phys. Chem. B* **2001**, *105*, 5599–5611.
(11) Gong, J.; Lipomi, D. J.; Deng, J.; Nie, Z.; Chen, X.; Randall, N. X.; Nair, R.; Whitesides, G. M. *Nano Lett.* **2010**, *10*, 2702–2708.
(12) Stoddart, P. R.; Cadusch, P. J.; Boyce, T. M.; Erasmus, R. M.; Comins, J. D. *Nanotechnology* **2006**, *17*, 680–686.
(13) Fang, Y.; Seong, N.-H.; Dlott, D. D. *Science* **2008**, *321*, 388–392.
(14) Sriram, S.; Bhaskaran, M.; Kostovski, G.; Mitchell, D. R. G.; Stoddart, P. R.; Austin, M. W.; Mitchell, A. *J. Phys. Chem. C* **2009**, *113*, 16610–16614.
(15) Braun, G.; Lee, S. J.; Dante, M.; Nguyen, T.-Q.; Moskovits, M.; Reich, N. *J. Am. Chem. Soc.* **2007**, *129*, 6378–6379.
(16) Huh, Y. S.; Chung, A.; Erickson, D. *Microfluid. Nanofluid.* **2009**, *6*, 285–297.
(17) Kostovski, G.; White, D. J.; Mitchell, A.; Austin, M. W.; Stoddart, P. R. *Biosens. Bioelectron.* **2009**, *24*, 1531–1535.
(18) Huh, Y. S.; Erickson, D. *Biosens. Bioelectron.* **2010**, *25*, 1240–1243.
(19) Weaver, M. J.; Zou, S.; Chan, H. Y. H. *Anal. Chem.* **2000**, *72*, 38A–47A.
(20) Jayawardhana, S.; Kostovski, G.; Mazzolini, A. P.; Stoddart, P. R. *Appl. Opt.* **2011**, *50*, 155–162.
(21) Zhang, Y.; Zhang, Y.; Terrill, R. H.; Bohn, P. W. *Thin Solid Films* **1998**, *335*, 178–185.
(22) Itoh, T.; McCreery, R. L. *J. Am. Chem. Soc.* **2002**, *124*, 10894–10902.
(23) Joo, S.-W. *Bull. Korean Chem. Soc.* **2007**, *28*, 1405–1409.
(24) Li, S.; Wu, D.; Xu, X.; Gu, R. *J. Raman Spectrosc.* **2007**, *38*, 1436–1443.
(25) Liu, Y.-C. *Langmuir* **2002**, *18*, 174–181.
(26) Oklejas, V.; Sjostrom, C.; Harris, J. M. *J. Am. Chem. Soc.* **2002**, *124*, 2408–2409.
(27) Oklejas, V.; Sjostrom, C.; Harris, J. M. *J. Phys. Chem. B* **2003**, *107*, 7788–7794.
(28) Zhang, W.; Yeo, B. S.; Schmid, T.; Zenobi, R. *J. Phys. Chem. C* **2007**, *111*, 1733–1738.
(29) Yang, Z.; Aizpurua, J.; Xu, H. *J. Raman Spectrosc.* **2009**, *40*, 1343–1348.
(30) Zhang, W.; Cui, X.; Yeo, B.-S.; Schmid, T.; Hafner, C.; Zenobi, R. *Nano Lett.* **2007**, *7*, 1401–1405.
(31) Picardi, G.; Chaigneau, M.; Ossikovski, R.; Licitra, C.; Delapierre, G. *J. Raman Spectrosc.* **2009**, *40*, 1407–1412.
(32) Jung, U.; Müller, M.; Fujimoto, N.; Ikeda, K.; Uosaki, K.; Cornelissen, U.; Tuczek, F.; Bornholdt, C.; Zargarani, D.; Herges, R.; Magnussen, O. *J. Colloid Interface Sci.* **2010**, *341*, 366–375.
(33) Carron, K. T.; Hurley, L. G. *J. Phys. Chem.* **1991**, *95*, 9979–9984.
(34) Mani, A. A.; Schultz, Z. D.; Caudano, Y.; Champagne, B.; Humbert, C.; Dreesen, L.; Gewirth, A. A.; White, J. O.; Thiry, P. A.; Peremans, A. *J. Phys. Chem. B* **2004**, *108*, 16135–16138.
(35) Moskovits, M.; Suh, J. S. *J. Phys. Chem. C* **1984**, *88*, 5526–5530.
(36) Lu, L.; Xie, W.; Liang, S. *Curr. Appl. Phys.* **2011**, *11*, 1302–1306.
(37) Reinhard, B. M.; Sheikholeslami, S.; Mastroianni, A.; Alivisatos, A. P.; Liphardt, J. *Proc. Natl. Acad. Sci. U.S.A.* **2007**, *104*, 2667–2672.
(38) Claridge, S. A.; Schwartz, J. J.; Weiss, P. S. *ACS Nano* **2011**, *5*, 693–729.
(39) Nara, J.; Higai, S.; Morikawa, Y.; Ohno, T. *J. Chem. Phys.* **2004**, *120*, 6705–6711.
(40) Dhirani, A.-A.; Zehner, R. W.; Hsung, R. P.; Guyot-Sionnest, P.; Sita, L. R. *J. Am. Chem. Soc.* **1996**, *118*, 3319–3320.
(41) Wan, L.-J.; Terashima, M.; Noda, H.; Osawa, M. *J. Phys. Chem. B* **2000**, *104*, 3563–3569.
(42) Vattuone, L.; Rocca, M.; Restelli, P.; Pupo, M.; Boragno, C.; Valbusa, U. *Phys. Rev. B* **1994**, *49*, 5113–5116.

(43) Rocca, M.; Savio, L.; Vattuone, L.; Burghaus, U.; Palomba, V.; Novelli, N.; de Mongeot, F. B.; Valbusa, U.; Gunnella, R.; Comelli, G.; Baraldi, A.; Lizzit, S.; Paolucci, G. *Phys. Rev. B* **2000**, *61*, 213–2227.
(44) Morikawa, Y.; Liew, C. C.; Nozoye, H. *Surf. Sci.* **2002**, *514*, 389–393.
(45) Molina, L. M.; Hammer, B. *Chem. Phys. Lett.* **2002**, *360*, 264–271.
(46) Zheng, Y. B.; Yang, Y.-W.; Jensen, L.; Fang, L.; Juluri, B. K.; Flood, A. H.; Weiss, P. S.; Stoddart, J. F.; Huang, T. J. *Nano Lett.* **2009**, *9*, 819–825.
(47) Franco, I.; George, C. B.; Solomon, G. C.; Schatz, G. C.; Ratner, M. A. *J. Am. Chem. Soc.* **2011**, *133*, 2242–2249.
(48) Laibinis, P. E.; Whitesides, G. M.; Allara, D. L.; Tao, Y. T.; Parikh, A. N.; Nuzzo, R. G. *J. Am. Chem. Soc.* **1991**, *113*, 7152–7167.
(49) Kresse, G.; Furthmuller, J. *Phys. Rev. B* **1996**, *54*, 11169–11186.
(50) Perdew, J. P.; Chevary, J. A.; Vosko, S. H.; Jackson, K. A.; Pederson, M. R.; Singh, D. J.; Fiolhais, C. *Phys. Rev. B* **1992**, *46*, 6671–6687.
(51) Kresse, G.; Joubert, D. *Phys. Rev. B* **1999**, *59*, 1758–1775.
(52) Neugebauer, J.; Scheffler, M. *Phys. Rev. B* **1992**, *46*, 16067–16070.